

The Ccz1-Mon1-Rab7 module and Rab5 control distinct steps of autophagy

Krisztina Hegedűs^{a,†}, Szabolcs Takáts^{a,†,*}, Attila Boda^{a,†}, András Jipa^b, Péter Nagy^a, Kata Varga^b, Attila L. Kovács^a, and Gábor Juhász^{a,b,*}

^aDepartment of Anatomy, Cell and Developmental Biology, Eötvös Loránd University, Budapest H-1117, Hungary;

^bInstitute of Genetics, Biological Research Centre, Szeged H-6726, Hungary

ABSTRACT The small GTPase Rab5 promotes recruitment of the Ccz1-Mon1 guanosine exchange complex to endosomes to activate Rab7, which facilitates endosome maturation and fusion with lysosomes. How these factors function during autophagy is incompletely understood. Here we show that autophagosomes accumulate due to impaired fusion with lysosomes upon loss of the Ccz1-Mon1-Rab7 module in starved *Drosophila* fat cells. In contrast, autophagosomes generated in Rab5-null mutant cells normally fuse with lysosomes during the starvation response. Consistent with that, Rab5 is dispensable for the Ccz1-Mon1-dependent recruitment of Rab7 to PI3P-positive autophagosomes, which are generated by the action of the Atg14-containing Vps34 PI3 kinase complex. Finally, we find that Rab5 is required for proper lysosomal function. Thus the Ccz1-Mon1-Rab7 module is required for autophagosome-lysosome fusion, whereas Rab5 loss interferes with a later step of autophagy: the breakdown of autophagic cargo within lysosomes.

Monitoring Editor

Suresh Subramani
University of California,
San Diego

Received: Mar 31, 2016

Revised: Aug 15, 2016

Accepted: Aug 17, 2016

INTRODUCTION

Autophagy ensures the lysosomal degradation of self-material, including cytosol and organelles. During the main pathway, double-membrane autophagosomes serve as the transport vesicles (Mizushima *et al.*, 2008). Endocytosis delivers plasma membrane, including transmembrane receptors, and exogenous substances

taken up from the environment to lysosomes. Thus autophagy and endocytosis converge at the level of lysosomes, where degradation of cargo arriving from both routes takes place.

A critical event during these transport processes is vesicle maturation: how the newly formed vesicles acquire the molecular characteristics and protein complexes that establish their identity and determine the subsequent vesicle fusion events that often culminate in the lysosomal compartment. Several similarities between endosomes and autophagosomes are known. For example, both autophagosomes and endosomes are positive for phosphatidylinositol-3-phosphate (PI3P) due to localized vacuolar protein sorting 34 (Vps34) PI3 kinase activity, which we showed to be required for the generation of both types of vesicles in *Drosophila* larvae (Lindmo and Stenmark, 2006; Juhász *et al.*, 2008; Dooley *et al.*, 2014). Autophagosomes can also fuse with endosomes to give rise to hybrid organelles termed amphisomes, which then fuse with lysosomes (Filimonenko *et al.*, 2007; Rusten *et al.*, 2007; Fader and Colombo, 2009).

Small GTPases of the Ras-related protein in brain (Rab) family are critical regulators of membrane trafficking in eukaryotic cells. An active, GTP-bound Rab protein binds to various effectors that usually regulate vesicle motility and fusion with the proper membrane compartment (Stenmark, 2009). In the endocytic pathway, Rab5 associates with early endosomes and activates a Vps34-containing phosphoinositide 3-kinase complex that generates PI3P on the surface of these vesicles. PI3P-binding domains such as the Fab-1, YGL023, Vps27, and EEA1 (FYVE) domain promote recruitment to early

This article was published online ahead of print in MBoc in Press (<http://www.molbiolcell.org/cgi/doi/10.1091/mbc.E16-03-0205>) on August 24, 2016.

[†]These are co-first authors.

The authors declare no competing interests.

S.T. and G.J. designed experiments: K.H., S.T., A.B., A.J., P.N., K.V., and A.L.K. carried out experiments: K.H., S.T., A.L.K., and G.J. analyzed data: S.T. and G.J. drafted the manuscript. All authors commented on and approved the manuscript before submission.

*Address correspondence to: Szabolcs Takáts (sz.takats@ttk.elte.hu), Gábor Juhász (szmrt@elte.hu).

Abbreviations used: Atg, autophagy-related gene; Ccz1, caffeine, calcium, and zinc 1; FYVE, Fab-1, YGL023, Vps27, and EEA1; GEF, guanine nucleotide exchange factor; HOPS, homotypic fusion and vacuole protein sorting; Lamp, lysosomal-associated membrane protein; LTR, LysoTracker Red; Mon1, monensin sensitivity protein 1; PI3P, phosphatidylinositol-3-phosphate; Rab, Ras-related protein in brain; SNARE, soluble N-methylmaleimide-sensitive factor attachment protein receptor; UVRAG, ultraviolet radiation resistance-associated gene; Vps, vacuolar protein sorting; Y2H, yeast two-hybrid.

© 2016 Hegedűs, Takáts, Boda, *et al.* This article is distributed by The American Society for Cell Biology under license from the author(s). Two months after publication it is available to the public under an Attribution-NonCommercial-Share Alike 3.0 Unported Creative Commons License (<http://creativecommons.org/licenses/by-nc-sa/3.0>).

"ASCB®," "The American Society for Cell Biology®," and "Molecular Biology of the Cell®" are registered trademarks of The American Society for Cell Biology.

Supplemental Material can be found at:
<http://www.molbiolcell.org/content/suppl/2016/08/22/mbc.E16-03-0205v1.DC1.html>

endosomes. Of importance, several proteins, including the vesicle tethers early endosomal antigen 1 (EEA1) and Rabenosin-5, have both FYVE and Rab5-binding domains, indicating that multiple interactions may play a role in the recruitment of effectors (Stenmark, 2009). Similarly, the Rab7 guanine nucleotide exchange factor (GEF) monensin sensitivity protein 1 (Mon1)–caffeine, calcium, and zinc 1 (Ccz1) complex binds to both the GTP-bound form of endosomal Rab5 and PI3P (Poteryaev et al., 2010; Cabrera et al., 2014; Cui et al., 2014). Rab7 is then activated by this complex and promotes fusion of late endosomes and lysosomes.

Others and we have shown that recruitment of the soluble N-methylmaleimide-sensitive factor attachment protein receptor (SNARE) Syntaxin 17 is a critical step in autophagosome maturation because these vesicles acquire fusion competence this way (Itakura et al., 2012; Takats et al., 2013). Interaction of Syntaxin 17 with the homotypic fusion and vacuole protein sorting (HOPS) tethering complex ensures efficient fusion between autophagosomes and lysosomes (Jiang et al., 2014; Takats et al., 2014). HOPS is believed to be a Rab7 effector, and Rab7 was indeed found to promote the formation of degradative autolysosomes in cultured cells (Gutierrez et al., 2004; McEwan et al., 2015), although it remains to be established whether this protein is already present on autophagosomes before the fusion with lysosomes. In theory, the binding of HOPS to lysosomal Rab7 and autophagosomal Syntaxin 17 (and other factors,

such as phospholipids) may be sufficient for its tethering activity (Stroupe et al., 2006; Hickey et al., 2009; Jiang et al., 2014; Takats et al., 2014). In addition, autophagy-related gene 14 (Atg14), a Vps34 kinase complex subunit that is important for autophagosome formation, also functions as a tether and promotes autophagosome-lysosome fusion by directly binding to Syntaxin 17 (Diao et al., 2015).

In yeast, the fusion machinery differs somewhat from that of the animal cells because the SNAREs involved are not homologous (Dilcher et al., 2001; Ishihara et al., 2001; Ohashi and Munro, 2010). Still, autophagosome fusion with the vacuole (the equivalent of the lysosomal system in metazoan cells) requires HOPS, Ypt7/Rab7, and its GEF, the Mon1-Ccz1 complex (Rieder and Emr, 1997; Kim et al., 1999; Wang et al., 2002), and more recently, autophagosome-like structures were found to accumulate in yeast cells lacking the major Rab5 homologue Vps21 (Chen et al., 2014). Of interest, decreased Rab5 function attenuates the autophagic degradation of the pathogenic, mutant form of huntingtin in cultured human cells. This was attributed to impaired Vps34 lipid kinase activity and reduced formation of the Atg5-Atg12 conjugate, both of which are important for autophagosome formation (Ravikumar et al., 2008).

Thus the role of the Rab5-Ccz1-Mon1-Rab7 axis during autophagy is not clear. We set out to address this problem in the popular animal model *Drosophila*. Fruit flies offer certain advantages for such studies. First, there is only a single fly homologue of Rab5 (unlike in mammalian and yeast cells, which both have three different Rab5 proteins; Pereira-Leal and Seabra, 2001). Second, massive induction of autophagy is seen in the fat and liver tissue-like fat cells of starved larvae. Third, it is straightforward to carry out functional studies in mosaic animals, in which mutant cells are surrounded by control cells in the same tissue of the same animal, which reduces variability because one can compare the phenotype of neighboring control and loss-of-function cells (Mauvezin et al., 2014; Nagy et al., 2015). Using this system, we show that Ccz1, Mon1, and Rab7 are required for autophagosome-lysosome fusion in fat cells of starved animals independent of Rab5. Of interest, we find that Rab5 functions downstream of the Rab7 module by controlling a later step of autophagy: degradation of autophagic cargo within lysosomes.

RESULTS

Rab7 is important for autolysosome formation

To characterize Rab7's role in autophagy, we generated Rab7-null mutant flies by imprecise excision of the P-element EY10675. The resulting Rab7[d1] allele carries a 1025-base pair deletion, which removes most of the first protein-coding exon and the 5' untranslated region (UTR) of all three predicted Rab7 isoforms (Figure 1, A and B). Animals homozygous or hemizygous for Rab7[d1] showed late pupal lethality, similar to another knockout allele published during the course of our work (Cherry et al., 2013).

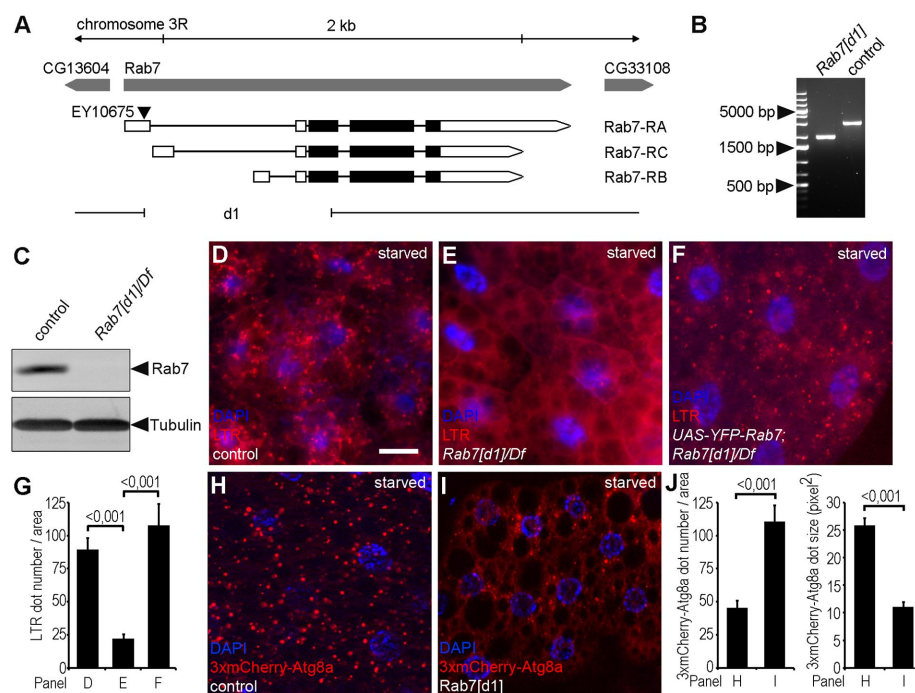


FIGURE 1: Rab7 is required for autophagy. (A) Genomic map of the *Rab7* locus, showing the exon-intron structure, including 5' and 3' UTRs (open bars). The *Rab7[d1]*-null allele was generated by imprecise excision of the P-element EY10675. The extent of the deletion is indicated by the gap in the line. (B) PCR amplification from the *Rab7* locus show the 1025-base pair deletion in *Rab7[d1]* mutants compared with controls. (C) Western blot shows the absence of Rab7 protein expression in samples prepared from larvae hemizygous for *Rab7[d1]*. Tubulin was used as loading control. (D–F) Many LTR-positive dots are present in fat cells of wild-type starved third-instar larvae (D). *Rab7* mutants show almost complete lack of LTR dots (E). This phenotype can be rescued by transgenic expression of Rab7 (F). (G) Quantification of data shown in D–F; $n = 10$ /genotype. (H, I) Large 3xmCherry-Atg8a-positive autolysosomes appear in starved control fat cells (H), whereas *Rab7* mutant cells contain more but smaller autophagic structures (I). (J) Quantification of data shown in H and I; $n = 10$ /genotype. Scale bar, 20 μ m (D–F, H, I). Error bars denote SE in G and J, and the numbers above the clasps show p values in these and all subsequent charts.

Western blots of third-instar larval lysates showed the absence of Rab7 protein in the mutant (Figure 1C), confirming that this allele represents a null mutant. Immunostaining developing eyes of control and Rab7[d1] mutant larvae revealed that down-regulation of endocytosed Notch and Boss receptors is impaired in Rab7 mutant tissue (Supplemental Figure S1, A, B, E, and F), consistent with the essential role of this protein for progression of late endosomes to endolysosomes.

To evaluate autophagy in our mutant, we stained fat cells of 4-h-starved, early L3-stage larvae with LysoTracker Red (LTR). LTR is an acidophilic dye commonly used for staining autolysosomes in this *Drosophila* tissue and detects many autolysosomes in control animals (Figure 1D). In contrast, Rab7 mutants showed a greatly reduced number of LTR-positive dots, which could be rescued by expressing YFP-Rab7 in the mutants (Figure 1, E–G). Because acidic

autolysosomes were absent from Rab7 loss-of-function fat cells, we tested whether earlier steps of the autophagic pathway are also affected. We used our novel, 3xmCherry-tagged Atg8a reporter driven by its endogenous promoter to find that the number of autophagic structures is increased and their average size is decreased in fat cells of starved Rab7 mutants compared with control animals (Figure 1, H–J). These data suggested that Rab7 is required for autolysosome formation in fat cells.

The Ccz1-Mon1-Rab7 module regulates autophagosome-lysosome fusion

In yeast and mammalian cells, Rab7 is activated by the Ccz1-Mon1 heterodimer, which acts as a GEF (Nordmann et al., 2010; Gerondopoulos et al., 2012). To confirm the existence of this complex in *Drosophila*, we carried out yeast two-hybrid (Y2H) experiments, which showed a strong interaction between these two proteins (Figure 2A). A recent *Drosophila* study demonstrated that both Mon1 and Ccz1 are required for Rab7 recruitment to endosomes (Yousefian et al., 2013). Thus the *Drosophila* Ccz1-Mon1 complex functions similarly to its yeast and mammalian homologues.

To evaluate the role of the Ccz1-Mon1 complex in autophagy, we first generated a Ccz1-null mutant line by imprecise excision of the P-element EY16389. The resulting Ccz1[d113] allele carries a 1644-base pair deletion that removes almost the entire coding region of this gene (Figure 2, B and C). We also obtained the recently published Mon1[d4]-null mutant *Drosophila* line (Yousefian et al., 2013) and investigated the effect of Ccz1 and Mon1 mutations on autophagy by LTR staining of fat cells from starved larvae. The lack of these genes strongly reduced the number of acidic autolysosomes (Figure 2, D, E, G, and I), and this phenotype could be rescued by expression of wild-type transgenes (Figure 2, F, H, and I), respectively. Mon1-null mutant fat cells of starved animals contained more but smaller 3xmCherry-Atg8a structures than did control cells (Supplemental Figure S2, A and B), similar to Rab7 mutants. In addition, Ccz1 and Mon1 mutant cells of the developing eye accumulated endocytosed but nondegraded Notch and Boss receptors, which is again similar to the situation in Rab7 mutants (Supplemental Figure S1, C, D, G, and H).

p62 (also known as Ref2P in flies) is a specific autophagic cargo commonly used to measure autophagic degradation (flux; Nezis et al., 2008; Pircs et al., 2012), along with the autophagosome-associated, lipidated form of Atg8a (Atg8a II). Western blots of lysates prepared from starved larvae showed that Rab7, Ccz1, and Mon1 mutants accumulate both p62 and Atg8a II (Figure 2J). A similar buildup of these proteins was seen in well-fed early-L3 and late-L3 wandering mutant larvae, respectively

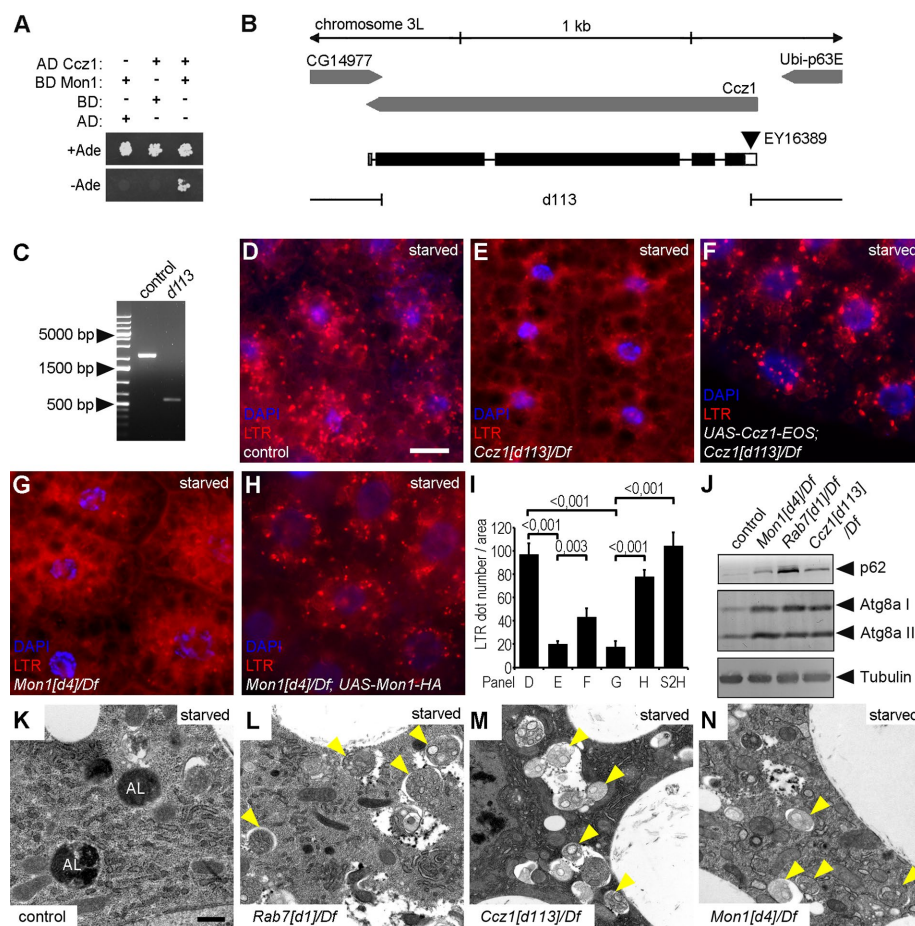


FIGURE 2: Rab7 module mutants are defective in autophagosome-lysosome fusion. (A) Y2H experiment shows the direct interaction of *Drosophila* Mon1 and Ccz1. (B) Genomic map of the Ccz1 locus. The Ccz1[d113] allele was generated by imprecise excision of the P-element EY16389. (C) PCR amplification of the Ccz1 locus shows the 1644-base pair deletion in Ccz1[d113] mutant animals relative to controls. (D–H) Many LTR-positive dots are seen in fat cells of starved control larvae (D). The formation of such acidic compartments is inhibited in Ccz1 (E) and Mon1 (G) mutants and can be restored by expression of wild-type Ccz1 and Mon1, respectively (F, H). (I) Quantification of LTR data shown in D–H and Supplemental Figure S2H; $n = 10$ /genotype. (J) Western blots from starved larvae reveal accumulation of the selective autophagic cargo p62 and lipidated, autophagosome-associated Atg8a II in Ccz1, Mon1, and Rab7 mutants. Tubulin serves as loading control. (K–N) Electron micrographs of fat cells dissected from starved third-instar larvae. Control cells (K) contain large, electron-dense autolysosomes (AL), whereas Rab7 module mutants (L–N) show accumulation of autophagosomes (arrowheads) and lack of autolysosomes. Scale bar, 20 μ m (in D, for D–H), 1 μ m (in K, for K–N).

(Supplemental Figure S2C). These results indicate that the Ccz1/Mon1/Rab7 module is required for autophagic degradation during starvation-induced basal and developmental autophagy.

We next tested the colocalization of the autophagy reporter 3xmCherry-Atg8a with lysosomal-associated membrane protein 1 (Lamp1)–green fluorescent protein (GFP), a marker for late endosomes and lysosomes. As expected, large autolysosomes were positive for both 3xmCherry-Atg8a and Lamp1 in wild-type cells (Supplemental Figure S2D). In contrast, the Lamp1-GFP and 3xmCherry-Atg8a structures were much smaller in animals lacking Rab7 or Ccz1, and their colocalization was strongly reduced (Supplemental Figure S2, E and F). In line with this, ultrastructural analysis of fat cells from starved larvae revealed that Rab7, Ccz1, and Mon1 mutants accumulate autophagosomes and that autolysosomes are absent from these cells, unlike control cells (Figure 2, K–N). Thus Rab7 and its GEF, the Ccz1-Mon1 complex, are required for autophagosome-lysosome fusion.

Ccz1-Mon1 recruits Rab7 to autophagosomes

Others and we have shown that a Syx17-Snap29-Vamp7 SNARE complex mediates autophagosome-lysosome fusion (Itakura *et al.*, 2012; Takats *et al.*, 2013), which is promoted by the HOPS tethering complex, an interacting partner of Syx17 (Jiang *et al.*, 2014; Takats *et al.*, 2014). Rab7 is known to localize to the lysosome (Bucci *et al.*, 2000). Because HOPS is considered to be an effector of Rab7, we reasoned that Rab7 must be present on autophagosomes. Indeed, 56% (112 of 200; $n = 10$) of dots positive for endogenous Atg8a colocalized with endogenous Rab7 in fat cells of starved control animals (Figure 3A). To confirm that these structures correspond to autophagosomes, we repeated this experiment using null mutants lacking Syx17 or an essential subunit of HOPS, Vps16A. These cells show large-scale accumulation of Atg8a-positive autophagosomes concentrated in the perinuclear region, as described earlier (Takats *et al.*, 2013, 2014), and 84% (168 of 200; $n = 10$) and 84.5% (169 of 200; $n = 10$) of Atg8a-positive structures overlapped with the Rab7 signal in Vps16A and Syx17 mutants (Figure 3, B and C), respectively. In contrast, the mutation of either Ccz1 or Mon1 prevented the colocalization of Atg8a

with Rab7: only 8% (16 of 200; $n = 10$) and 11% (22 of 200; $n = 10$) of the dots overlapped (Figure 3, D and E), respectively. We also carried out immunogold labeling to show that GFP-Rab7 is associated with the autophagosomal membrane (Figure 3F).

These data suggested that Rab7 is recruited to autophagosomes in a Ccz1-Mon1 (GEF)–dependent manner, independent of HOPS or Syx17. Of importance, a constitutively active, GTP-locked mutant form of Rab7 was detected on endogenous Atg8a-positive autophagosomes even in the absence of Mon1 (Supplemental Figure S2G), and Rab7-GTP expression rescued starvation-induced punctate LTR/autolysosome staining in Mon1 mutant fat cells (Supplemental Figure S2H and Figure 2I). This is in line with yeast genetic data, which showed that the vacuole fragmentation phenotype of yeast Ccz1 mutants can be suppressed by point mutations in Ypt7/Rab7 (Kucharczyk *et al.*, 2001).

Rab5 is dispensable for autophagosome-lysosome fusion

Rab5 promotes the recruitment of the Ccz1-Mon1 complex to endosomal membranes. Because Ccz1 and Mon1 are both required for the autophagosomal localization of Rab7 and the subsequent fusion to lysosomes, we asked whether Rab5 plays a role in this process. We first confirmed that the *Drosophila* Ccz1-Mon1 complex preferentially binds to GTP-locked Rab5 and GDP-locked Rab7 in Y2H experiments (Figure 4A). Next we generated mosaic animals expressing the 3xmCherry-tagged Atg8a reporter in all cells and containing clones of cells homozygous for Rab5[d2], a widely used null mutant allele (Wucherpennig *et al.*, 2003). Surprisingly, Rab5 mutant cells (marked by the expression of GFP) contained large 3xmCherry-Atg8a-positive dots in similar numbers and size as surrounding control cells did after a 4-h starvation (Figure 4, B and C). Because these autophagic structures colocalized with lysosomal Lamp1-GFP (Figure 4D), this suggested that autophagosomes normally fuse with lysosomes to generate autolysosomes in the absence of Rab5. We further confirmed these findings by ultrastructural analysis of Rab5 mutant fat cell clones, which also revealed the presence of large, electron-dense autolysosomes and no accumulation of autophagosomes (Figure 4E and Supplemental Figure S3A). In line with this, Rab5 was dispensable for the recruitment of GFP-Rab7 to autophagic structures labeled by 3xmCherry-Atg8a (Figure 4F). It is worth noting that the cytoplasmic signal of GFP-Rab7 is slightly elevated in starved Rab5-null mutant fat cell clones (Figure 4F and Supplemental Figure S3B). We also tested the colocalization of Rab7 with the late endosome and lysosome marker Lamp, using our new reporter: endogenous promoter-driven, full-length *Drosophila* dLamp-3xmCherry. In fat cells of well-fed animals that show minimal autophagic activity, loss of Rab5 caused a striking decrease in the number of GFP-Rab7 and dLamp-3xmCherry vesicles relative to surrounding wild-type cells, which contain abundant Lamp1- and Rab7-positive dots that often overlap (Supplemental Figure S3C). However, in starved animals, many colocalizing GFP-Rab7 and dLamp-3xmCherry vesicles formed in Rab5 mutant cells (Supplemental Figure S3D), potentially due to the induction of autophagy.

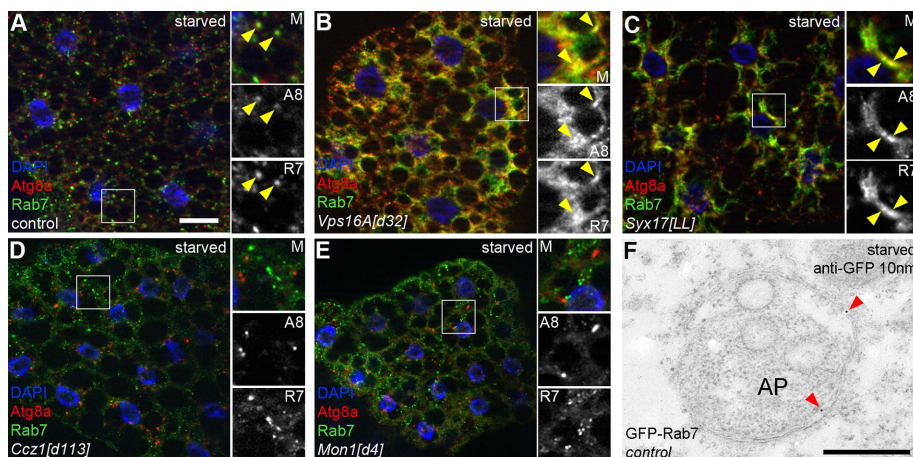


FIGURE 3: The Mon1-Ccz1 complex is necessary for Rab7 recruitment to autophagic structures. (A–E) Endogenous Atg8a and Rab7 immunolabeling of fat cells in starved larvae. Insets, boxed areas enlarged (M, merged image; A8, Atg8a channel; R7, Rab7 channel; arrowheads mark colocalization). Colocalizing dots are seen in wild-type larvae (A). The Atg8a and Rab7 signals largely overlap in the perinuclear regions of Vps16A (B) and Syx17 (C) mutant fat cells. Loss of Ccz1 (D) or Mon1 (E) prevents the colocalization of Rab7 and Atg8a. (F) Immuno-electron microscopy shows that GFP-Rab7 is associated with the surface of an autophagosome (AP). Immunogold particles are highlighted by arrowheads. Scale bar, 20 μm (in A, for A–E), 0.5 μm (F).

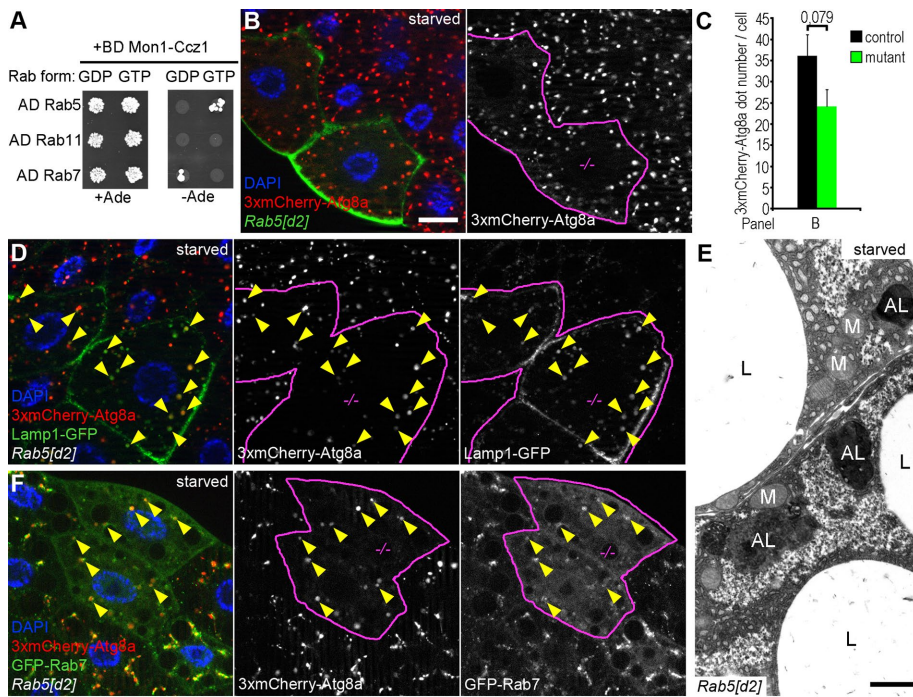


FIGURE 4: Rab5 is dispensable for autophagosome-lysosome fusion. (A) Y2H assays show that the Mon1-Ccz1 complex interacts with GTP-bound Rab5 and GDP-bound Rab7. Rab11 was used as negative control. (B) GFP-positive fat cell clones homozygous for the *Rab5[d2]*-null mutation show a similar pattern of 3xmCherry-Atg8a granules as seen in GFP-negative control cells. (C) Quantification of data shown in B; $n = 10$ /genotype. (D) 3xmCherry-Atg8a and Lamp1 colocalize in intracellular structures (arrowheads) in *Rab5* mutant clones, and the accumulation of Lamp1-GFP in vesicles and at the plasma membrane is obvious in *Rab5[d2]* cells. (E) Large, dense autolysosomes (ALs) are visible in an electron micrograph from a *Rab5* mutant fat cell of a starved larva. L, lipid droplet; M, mitochondrion. (F) 3xmCherry-Atg8a colocalizes with GFP-Rab7 (arrowheads) in starved *Rab5* mutant clone cells, and the diffuse cytoplasmic level of Rab7 is increased in mutant cells. Scale bar, 20 μ m (B, D, F). Clone cells in grayscale images of D and F are outlined in magenta. Note that *Rab5* mutant cells were recognized based on their larger size and nucleus and different reporter expression pattern in D and F. See also Figure 7B and Supplemental Figure S3B for further data. Scale bar, 1 μ m (E).

We noticed that *Rab5* mutant fat cells are larger than neighboring control cells, which is in line with a report showing that the loss of *Rab5* function confers a selective growth advantage in cells of the developing wing (Lu and Bilder, 2005). We carried out epistasis analysis to find out how the different phenotypes behave in *Rab5* and *Mon1* double-mutant cells. First, we performed LTR staining of fat cells from starved larvae containing *Rab5* or *Mon1* single-mutant and *Rab5*/*Mon1* double-mutant clones. We found that cells homozygous for *Rab5[d2]* contain large LTR-positive autolysosomes with similar size and number as in surrounding control cells (Supplemental Figure S4, A and D). In contrast, *Mon1[d4]* mutant clones had fewer and fainter acidic, LTR-positive structures (Supplemental Figure S4, B and D). Double-mutant fat cells lacking both *Rab5* and *Mon1* appeared similar to *Mon1* single-mutant cells regarding the lack of LTR dots (Supplemental Figure S4, C and D). Ultrastructural analysis revealed the accumulation of autophagosomes and lack of autolysosomes in double-mutant cells (Supplemental Figure S4E), as seen in *Mon1* single mutants (Figure 2N). In addition, both *Rab5* single- and *Rab5*/*Mon1* double-mutant cells are larger than neighboring control cells, unlike *Mon1* single-mutant clone cells, which have a normal size (Supplemental Figure S4, A–C).

Taken together, our results indicate that the autophagosome fusion defect of *Ccz1*/*Mon1*/*Rab7* module mutants is independent of

Rab5, whereas the large-cell size phenotype caused by *Rab5* deletion is epistatic to the mutation of *Mon1*.

Rab5 is dispensable for the generation of PI3P-positive autophagosomes

The *Ccz1*-*Mon1* complex strongly binds to membrane lipids, including PI3P (Poteryaev et al., 2010; Cabrera et al., 2014), which is enriched in early endosomal and autophagosomal membranes. To test whether *Drosophila* *Mon1* also has an affinity for PI3P, we purified recombinant *Mon1* and performed a protein-lipid overlay assay. Indeed, *Mon1* bound to PI3P with high affinity, among other phospholipids (Figure 5A). These data raised the possibility that the *Ccz1*-*Mon1* complex is recruited to autophagosomes through binding to PI3P.

We showed previously that the *Vps34* lipid kinase complex is required for the generation of PI3P-positive endosomes and autophagosomes in *Drosophila* fat cells (Juhasz et al., 2008). *Vps34* is activated by *Rab5* on endosomes (Stenmark, 2009). In the present study, we found that autophagosome-lysosome fusion takes place in the absence of *Rab5*. Thus autophagosomal PI3P may be generated during autophagy induction in *Rab5* mutant fat cells. We already showed that the PI3P reporter GFP-FYVE labels mostly endosomes in well-fed larval fat cells, whereas starvation results in the generation of autophagosomes that are also positive for GFP-FYVE (Juhasz et al., 2008). We quantified the autophagosomal localization of GFP-FYVE using our 3xmCherry-Atg8a reporter in fat cells of nutrient-replete and -starved animals. PI3P-positive structures very rarely colocalized with 3xmCherry-Atg8a in well-fed cells (9.5%; 19 of 200; $n = 10$), whereas during starvation, 89.5% (179 of 200; $n = 10$) of 3xmCherry-Atg8a vesicles were positive for PI3P (Supplemental Figure S5). This is likely explained by the metabolic and storage functions of the fat body in *Drosophila*, as starvation-induced inactivation of TOR kinase in fat cells not only triggers autophagy but also down-regulates endocytosis (Hennig et al., 2006).

In line with the importance of *Rab5* for endocytic maturation, the loss of *Rab5* completely suppressed PI3P generation in well-fed cells, based on the lack of GFP-FYVE puncta formation (Figure 5, B and D). However, GFP-FYVE-positive structures appeared in *Rab5* mutant cells in similar numbers as in control cells during starvation (Figure 5, C and D). This is in line with the rest of our data and indicates that PI3P is generated on autophagosomes independently of *Rab5*.

Two multisubunit *Vps34* PI3 kinase complexes exist, which share three core subunits: the catalytic subunit, *Vps34*; the regulatory subunit, *Vps15*; and *Atg6* (Beclin1). The mutually exclusive subunits that define the two distinct complexes are ultraviolet radiation resistance-associated gene (UVRAG) and *Atg14*, respectively

Atg14, but not ultraviolet radiation resistance-associated gene, supports PI3P-positive autophagosome formation in starved fat cells

Two multisubunit *Vps34* PI3 kinase complexes exist, which share three core subunits: the catalytic subunit, *Vps34*; the regulatory subunit, *Vps15*; and *Atg6* (Beclin1). The mutually exclusive subunits that define the two distinct complexes are ultraviolet radiation resistance-associated gene (UVRAG) and *Atg14*, respectively

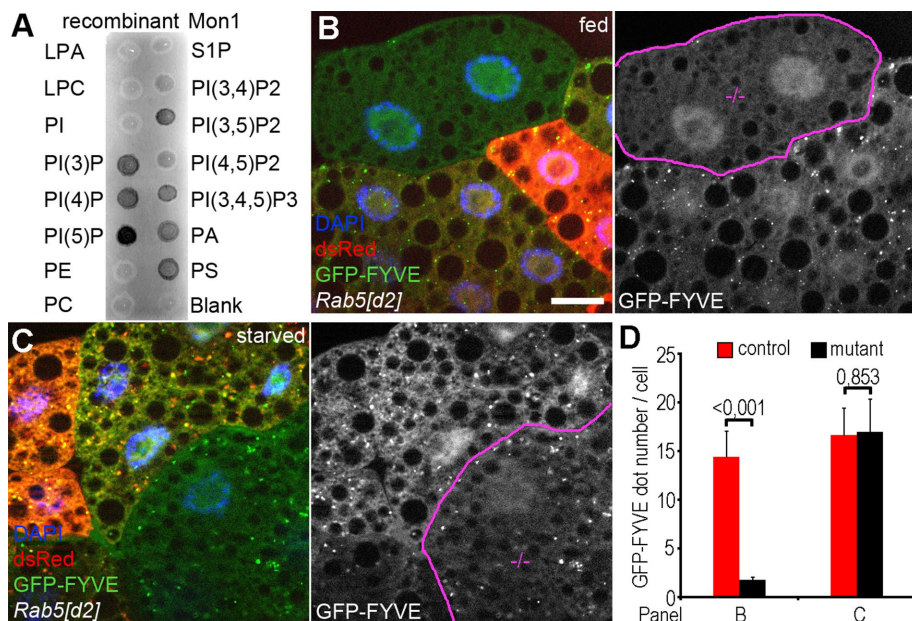


FIGURE 5: Autophagosomal PI3P generation is independent of Rab5. (A) Mon1 binds to several phospholipids, with a preference for phosphatidylinositol monophosphates, including PI3P. (B) GFP-FYVE labels PI3P-positive endosomes in fat cells of well-fed larvae, which are almost completely absent from dsRed-negative *Rab5* mutant clone cells. (C) GFP-FYVE dots are observed in large numbers during starvation in both *Rab5[d2]* homozygous mutant (dsRed⁻) and control (dsRed⁺) cells. (D) Quantification of data shown in B and C; *n* = 10/genotype. Clone cells in grayscale images of B and C are outlined in magenta. Scale bar, 20 μ m (in B, for B, C). LPA, lysophosphatidic acid; LPC, lysophosphocholine; PA, phosphatidic acid; PC, phosphatidylcholine; PE, phosphatidylethanolamine; PI, phosphatidylinositol; PS, phosphatidylserine; S1P, sphingosine-1-phosphate.

(Itakura *et al.*, 2008; Matsunaga *et al.*, 2009). It is clear that Atg14 functions during autophagosome biogenesis in yeast (Obara *et al.*, 2006), but both proteins were suggested to regulate autophagy in mammalian cells (Liang *et al.*, 2006; Itakura *et al.*, 2008).

We recently reported that UVRAG is dispensable for autophagosome formation and fusion with lysosomes in *Drosophila* fat cells (Takats *et al.*, 2014). To clarify the role of the Atg14 and UVRAG complexes during PI3P formation, we targeted the Atg14 locus using Cas9 mutagenesis. A 790-base pair deletion was identified that begins 17 base pairs upstream of the start ATG and deletes nearly the first half of the protein-coding sequence (Supplemental Figure S6, A and B). Flies homozygous for this Atg14[d13] allele accumulated high amounts of the specific autophagic cargo p62, and mutant fat cell clones completely lacked LTR-positive autolysosomes (Supplemental Figure S6, C and D), similar to previously described Atg mutants. Of importance, the expression of an endogenous promoter-driven, C-terminally hemagglutinin (HA)-tagged Atg14 transgene on the Atg14 mutant background suppresses the buildup of p62 (Supplemental Figure S6C), indicating that the autophagy defect is solely due to loss of Atg14 in these animals.

We used our new Atg14[d13] and the recently described UVRAG-null mutant (Takats *et al.*, 2014) alleles to test how these affect Vsp34 kinase activity and autophagy. UVRAG[LL] mutant fat cells showed a complete lack of PI3P under well-fed conditions (Figure 6, A and G), whereas starvation readily induced GFP-FYVE dots both in control and UVRAG loss-of-function cells (Figure 6, B and G). Cells lacking Atg14 showed an opposite phenotype: the number of GFP-FYVE structures was not statistically significantly different from that in neighboring control cells in the fed state (Figure 6, C and G), whereas upon starvation, the generation of

PI3P-positive vesicles was strongly decreased in Atg14[d13] mutant clones (Figure 6, D and G). We also tested whether the formation of 3xmCherry-Atg8a-positive structures is affected in UVRAG and Atg14 mutants. In cells lacking UVRAG, the number of 3xmCherry-Atg8a dots was comparable to that in control cells (Figure 6, E and H), in line with our recent report. In contrast, autophagic structures were absent from Atg14 mutant fat cell clones (Figure 6, F and H). We also tested the autophagosomal localization of Mon1 in wild-type and mutant backgrounds to more directly support these findings. As expected, we detected the presence of Mon1-HA on endogenous Atg8a-positive autophagosomes in both control and UVRAG mutant fat cells (Supplemental Figure S6, E and F). In contrast, Atg14 mutant cells lacked endogenous Atg8a-positive autophagosomes, whereas Mon1-HA dots were still observed (Supplemental Figure S6G).

Finally, we tested the level of p62 in fed and starved larvae in two independent UVRAG-null mutant lines, as well as in Atg14[d13] homozygotes. We found large-scale accumulation of p62 in Atg14 mutants under both conditions (Figure 6I), the results together indicating that the Atg14 complex is required for PI3P-positive autophagosome formation. UVRAG loss-of-function

lines showed a moderate increase of p62 compared with control animals (Figure 6I). These findings are consistent with a recent study in which we showed that although the loss of UVRAG does not inhibit autophagosome formation or fusion, it impairs the lysosomal degradation of autophagic cargo (Takats *et al.*, 2014), which is likely responsible for the increase in the amount of p62. Considering that UVRAG- but not Atg14-defective cells showed very similar phenotypes regarding GFP-FYVE distribution and 3xmCherry-Atg8a puncta formation to the ones observed in *Rab5* mutants, we propose that *Rab5* regulates endosomal traffic through an UVRAG-containing Vps34 complex in *Drosophila* fat cells. Moreover, *Rab5* is dispensable for the activity of the Atg14-containing Vps34 complex, which promotes autophagosome formation.

Rab5 facilitates autophagic cargo degradation by regulating lysosomal function

Considering our recent findings that UVRAG regulates endocytosis and lysosomal function (Takats *et al.*, 2014) and that *Rab5* appears to act on endosomal membrane trafficking at least in part through the Vps34-UVRAG complex, we hypothesized that *Rab5* may also have a role in maintaining proper lysosomal function. To evaluate autophagic degradation (flux) in *Rab5* mutants, we generated a novel, tubulin promoter-driven GFP-p62 reporter. Because the tubulin promoter is insensitive for autophagy induction signals, unlike that of endogenous p62, it ensures a constant and relatively low expression level in fat cells, so this reporter may be even better for measuring autophagic flux than the endogenous protein. An elevated level of GFP-p62 was seen in *Rab5[d2]* homozygous cell clones compared with neighboring control cells (Figure 7, A and A').

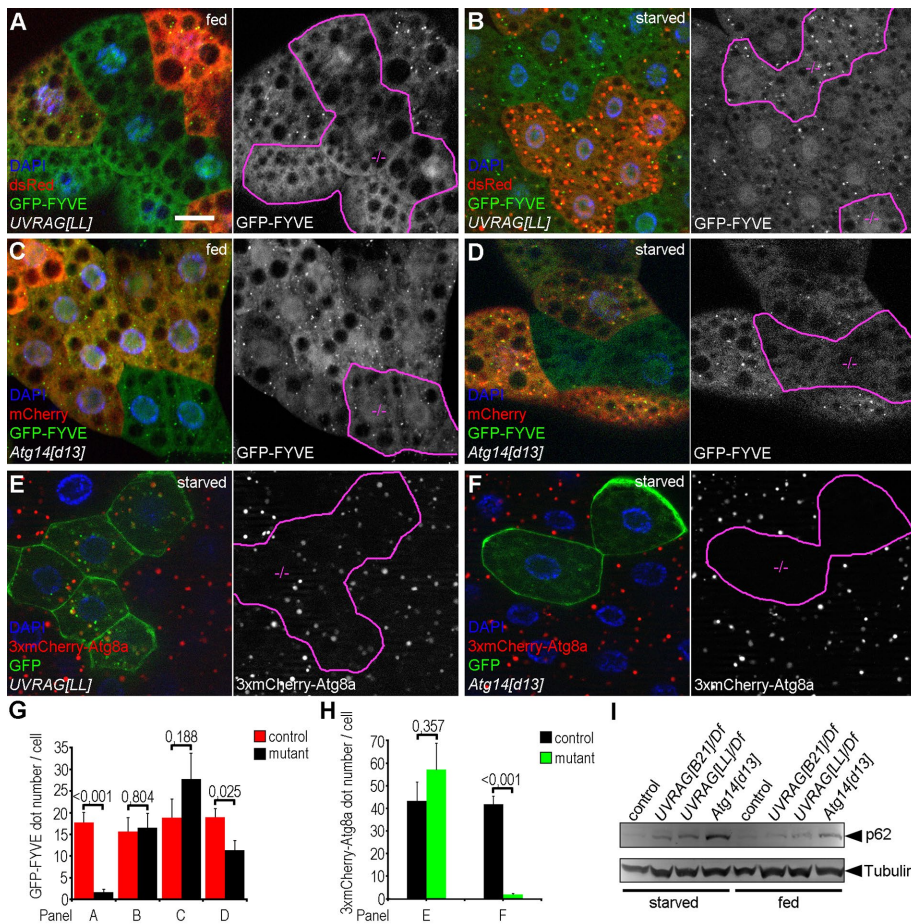


FIGURE 6: Different mechanisms of endosomal and autophagosomal PI3P formation. (A, B) GFP-FYVE–marked, PI3P-positive endosomes are absent from *UVRAG* mutant fat cell clones (dsRed– cells in A) of well-fed L3 larvae. However, starvation induces the generation of GFP-FYVE dots in *UVRAG* loss-of-function cells (dsRed–) in a similar number as in dsRed+ controls (B). (C, D) The number of GFP-FYVE–positive endosomes is similar in well-fed *Atg14* mutant clones (dsRed–) and dsRed+ control cells (C). In contrast, *Atg14* mutant cells contain fewer GFP-FYVE dots than control cells under starvation conditions (D). (E) Starvation-induced formation of 3xmCherry-Atg8a–labeled autophagic structures is similar in *UVRAG*–null mutant clones (GFP+) and control cells (GFP–). (F) On the contrary, complete inhibition of punctate 3xmCherry-Atg8a is observed in GFP+ *Atg14* mutant cells compared with neighboring GFP–controls. (G, H) Quantification of data in A–D (G) and E–F (H); $n = 10$ /genotype. (I) Western blots reveal that *UVRAG* mutants show mild, whereas *Atg14* mutants show strong, accumulation of the autophagic cargo p62 in both well-fed and starved larvae. Tubulin serves as a loading control. Clone cells in grayscale images of A–F are outlined in magenta. Scale bar, 20 μ m (in A, for A–F).

To test whether this is due to impaired lysosomal digestion, we measured the level of Lamp1-GFP, a reporter that consists of GFP linked to only one transmembrane domain followed by the cytoplasmic tail of human Lamp1 protein. As a result, GFP is constantly degraded within lysosomes, and thus its levels inversely correlate with lysosome function (Pulipparacharuvil *et al.*, 2005). Rab5 mutant clones showed a large-scale accumulation of Lamp1-GFP on intracellular structures and in the plasma membrane relative to surrounding control cells (Figure 7B). Of interest, vesicles positive for dLamp-3xmCherry are fainter in Rab5-null mutant cells than in control cells (Supplemental Figure S3, C and D). This is likely because in this case, full-length *Drosophila* dLamp protein is tagged with 3xmCherry on its C-terminus facing the cytoplasm, so this reporter is better suited for following trafficking to, but not turnover in, lysosomes. These data taken together indicate defective trafficking and turnover of lysosomal membrane proteins in Rab5 mutant

cells. Finally, we examined the activity of the lysosomal hydrolase cathepsin B by incubating fat cells dissected from starved larvae in a medium containing its substrate Magic Red. In control cells, Magic Red penetrates into cells and stains degrading lysosomes that contain active cathepsin B. Rab5 mutant fat cells showed highly reduced cathepsin B activity (Figure 7C), further supporting our model that Rab5 promotes the degradation of autophagic cargo by facilitating the targeting of lysosomal proteins.

Of note, the Rab7 module also appears to promote lysosomal function because the lysosomal processing of pro–cathepsin L was clearly perturbed in Mon1, Rab7, and Ccz1 mutant animals (Figure 7D). Mon1 and Rab7 loss-of-function fat cells of starved larvae showed the accumulation of small Lamp1-GFP or dLamp-3xmCherry puncta compared with surrounding control cells (Figure 7, E and F, and Supplemental Figure S7, A and B), which likely represent primary lysosomes that are unable to fuse with autophagosomes. Of interest, this phenotype is clearly different from that seen in Rab5 mutant cells, which showed large-scale accumulation of Lamp1-GFP in large autolysosomes and at the plasma membrane (Figure 7B). These observations again support that Rab5 and Rab7 modules play different roles during autophagy, as well as in lysosomal membrane protein trafficking and turnover.

DISCUSSION

In this study, we show that the Rab7 module and Rab5 control different steps of autophagy. Rab7 mediates autophagosome-lysosome fusion together with its GEF, the Ccz1-Mon1 complex. This is likely achieved by the recruitment of Rab7 to autophagosomes in a Ccz1-Mon1–dependent manner. Although *Drosophila* Mon1 binds to the active, GTP-locked form of Rab5 as in other organisms (Poteryaev *et al.*, 2010; Cabrera

et al., 2014), Rab5 is dispensable for the fusion of autophagosomes with lysosomes and for Rab7 localization to autophagosomes and autolysosomes. The question is then: what is the signal that recruits Ccz1-Mon1 and Rab7 to autophagic structures?

Mon1 and Ccz1 bind to phospholipids, including PI3P, in yeast (Cabrera *et al.*, 2014), and we find that *Drosophila* Mon1 has similar features. This raises the possibility that the Ccz1-Mon1 complex is recruited to the PI3P-positive surface of autophagosomes through this interaction. Vps34-dependent PI3P generation is required for autophagosome formation and endosome maturation. Vps34 is activated by Rab5 (Stenmark, 2009). Of interest, our data suggest that loss of Rab5 inhibits PI3P generation only on endosomes but not on autophagosomes. Loss of *UVRAG* but not *Atg14* inhibits PI3P generation on endosomes, whereas loss of *Atg14* leads to complete inhibition of PI3P-positive autophagosome biogenesis. Thus *UVRAG* is dispensable for Vps34 activity during

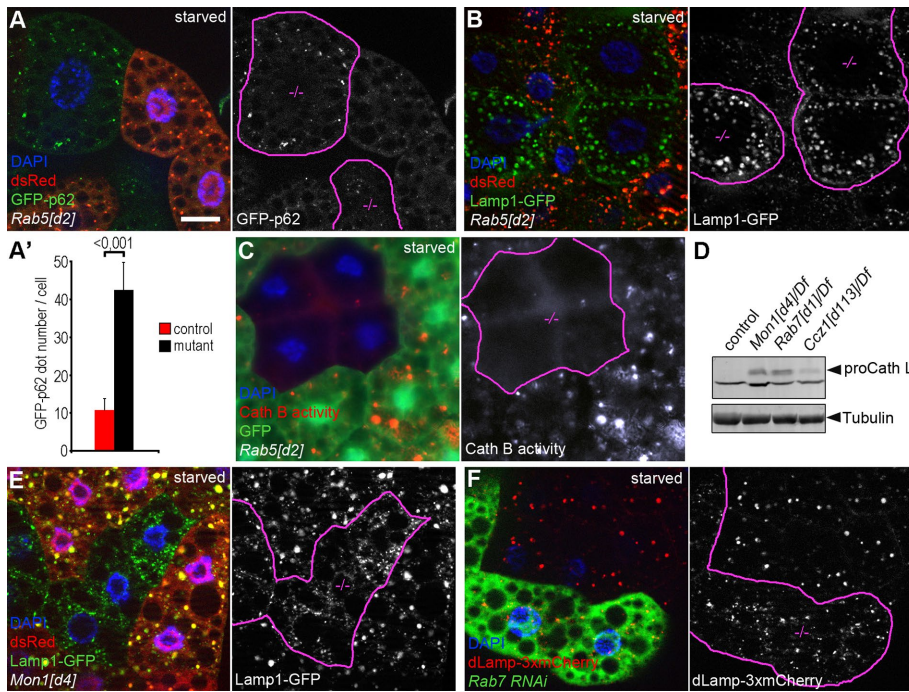


FIGURE 7: Rab5 is required for proper autolysosomal degradation. (A) The selective autophagic cargo p62 accumulates in *Rab5* mutant (*dsRed*[−]) clones compared with *dsRed*⁺ control cells. Note that GFP-p62 is expressed in all cells by the constitutive tubulin promoter, which excludes transcriptional changes. (A') Quantification of data shown in A; *n* = 10/genotype. (B) In *Rab5* mutant clone cells (*dsRed*[−]), the late endosomal and lysosomal marker Lamp1-GFP accumulates both intracellularly and at the plasma membrane compared with surrounding *dsRed*⁺ control cells. (C) Strongly reduced cathepsin B activity is observed in GFP[−] *Rab5* mutant clone cells compared with GFP⁺ control cells. (D) Western blot reveals the obvious accumulation of pro-cathepsin L in lysates of *Rab7*, *Ccz1*, and *Mon1* mutant larvae compared with controls. (E) In contrast to *dsRed*⁺ control cells, *dsRed*[−] *Mon1* mutant clones show highly fragmented Lamp1-GFP positive lysosomes. (F) Similarly, the dLamp-3xmCherry compartment is dispersed in *Rab7* RNAi clones (GFP⁺) compared with surrounding GFP[−] control cells. Clone cells in grayscale images of A–C, E, and F are outlined in magenta. Scale bar, 20 μm (in A, for A–C, E, F).

autophagosome formation, and its loss causes a defect in autolysosomal degradation (Takats *et al.*, 2014). Similarly, *Rab5* mutant cells showed accumulation of autophagic cargo due to impaired lysosomal degradation.

Recently the *Rab5*-related Vps21 small GTPase was suggested to control the fusion of autophagosome with the vacuole (lysosome) in yeast cells (Chen *et al.*, 2014). In this study, clusters of autophagic structures were found to accumulate near the vacuole. However, these vesicles were positive for both the autophagy marker GFP-Atg8 and the vacuolar marker FM4-64, suggesting that some sort of fusion must have occurred in this case, too.

On the basis of our results, we propose the following model of autolysosome formation in fat cells of starved *Drosophila* larvae (Figure 8). PI3P-positive autophagosomes are generated through the action of an Atg14-containing Vps34 PI3 kinase complex. PI3P attracts Ccz1-Mon1, which promotes *Rab7* recruitment to autophagosomes. Both PI3P and *Rab7* bind to the HOPS tethering complex, and thus these factors promote the tethering of autophagosomes with late endosomes and lysosomes. The membrane fusion is then executed by the Syx17-Snap29-Vamp7 SNARE complex. Autophagic cargo is broken down in autolysosomes, and their full degradative capacity requires the function of *Rab5* and the UVRAG-containing Vps34 complex for the proper delivery of lysosomal proteins, likely including both acidic hydrolases and membrane proteins. This is in line with the finding that simultaneous knockdown of all three

Rab5 homologues leads to a collapse of the endolysosomal system in mouse liver cells (Zeigerer *et al.*, 2012).

Others and we have already demonstrated that autophagosome-lysosome fusion is mediated by the HOPS tethering complex and the SNAREs Syx17, Snap29, and Vamp7/8 (Itakura *et al.*, 2012; Takats *et al.*, 2013, 2014; Jiang *et al.*, 2014). It is not yet clear how these fusion factors are recruited to the autophagosomal membrane. HOPS is known as a *Rab7* effector (Stenmark, 2009), and according to our findings, *Rab7* is present on autophagosomes. We propose that autophagosomal PI3P recruits the Ccz1-Mon1-*Rab7* module to facilitate the loading of HOPS and subsequent tethering of vesicles.

Vps34 is considered as a bona fide *Rab5* effector (Stenmark, 2009). Surprisingly, we found that whereas *Rab5* mediates only the generation of PI3P on endosomes mainly through the action of a UVRAG-containing Vps34 complex, it is dispensable for PI3P-positive autophagosome biogenesis, which depends on the Atg14-containing Vps34 complex. Thus the current concept that Vps34 is a *Rab5* effector must be revisited: it is true for endocytosis but not applicable for autophagy in fat cells of starved *Drosophila* larvae.

A previous study showed that *Rab5* promotes autophagy-mediated huntingtin clearance in cultured human cells and *Drosophila* eyes (Ravikumar *et al.*, 2008). Simultaneous small interfering RNA knockdown of all three *Rab5* genes (*Rab5a*,

Rab5b, *Rab5c*) reduced the level of Atg5-Atg12 conjugate and autophagosome formation. Although we did not see perturbations of autophagosome biogenesis and fusion in *Rab5* mutant fat cells, these discrepancies may be due to the different models used. In our experiments, starvation induces a massive wave of autophagy in larval *Drosophila* fat cells that entirely relies on the activity of the *Rab5*-independent Atg14-Vps34 PI3 kinase complex. It is possible that during the basal, nonstarved conditions studied by Ravikumar *et al.* (2008), *Rab5* can contribute to autophagosome formation. In fact, UVRAG has also been suggested to control autophagosome formation in cultured cells, which is compatible with this model (Liang *et al.*, 2006).

In summary, *Rab7* is recruited to autophagosomes by the Ccz1-Mon1 complex to promote autophagosome-lysosome fusion. We show that autophagosome formation and fusion is independent of *Rab5* and the UVRAG-containing Vps34 PI3 kinase complex but requires the action of the Atg14-Vps34 complex. *Rab5*, similar to UVRAG, is necessary for proper lysosomal function by promoting the trafficking of lysosomal proteins.

MATERIALS AND METHODS

Fly work

Flies were kept on standard yeast/cornmeal medium. For starvation experiments, well-fed mid L3-stage larvae (aged 80–88 h after egg laying) were floated in a 20% sucrose solution for 4 h. The *Rab7[d1]*

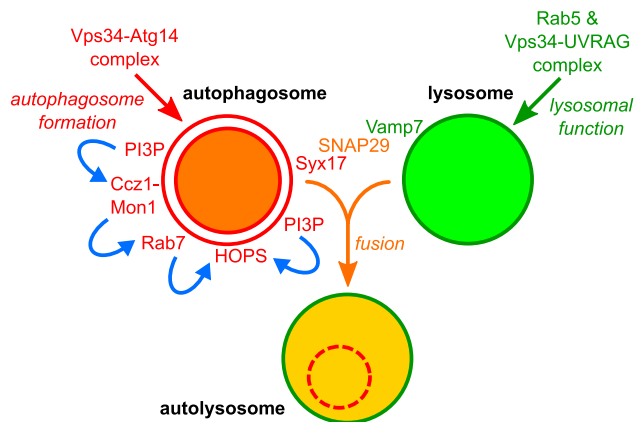


FIGURE 8: Proposed model of autophagosome maturation. PI3P is a key membrane lipid regulating both endocytosis and autophagy, the two main lysosomal degradation pathways. Rab5, together with its effector, the Vps34-UVRAG complex, promotes endosomal maturation and proper degradative capacity of lysosomes through the generation of PI3P on endosomal membranes. In parallel, the Vps34-Atg14 complex produces PI3P during autophagosome formation in a Rab5-independent manner. PI3P-positive autophagosomes mature to gain fusion competence by acquiring Rab7 via the action of the PI3P-binding Ccz1-Mon1 GEF complex. Both Rab7 and PI3P are likely important for recruiting the HOPS tethering complex to promote autophagosome-lysosome fusion, together with the Syx17-Snap29-Vamp7 SNARE complex.

and *Ccz1[d113]* null alleles were generated by imprecise excision of the transposable elements *Rab7[*EY10675*]* and *Ccz1[*EY16389*]*, respectively (both obtained from the Bloomington *Drosophila* Stock Center [BDSC], Bloomington, IN). The *Atg14[d13]* allele was generated by clustered regularly interspaced short palindromic repeats/Cas9 mutagenesis using a double gRNA approach as described previously (Kondo and Ueda, 2013). In all three cases, null mutant lines were identified by PCR screening and sequencing of candidates. The deficiencies *Df(3R)Exel6196*, *Df(3L)Exel6098*, and *Df(2L)ED7853* were obtained from BDSC and *Df(2L)ED784* from *Drosophila* Genomics and Genetic Resources (Kyoto, Japan). *UAS-YFP-Rab7*, *UAS-YFP-Rab7[Q67L]*, *UAS-GFP-Rab7*, *hs-Gal4*, *da-Gal4*, and the *Rab5*-null mutant *FRT40A Rab5[d2]* lines came from BDSC. The RNA interference line *UAS-Rab7[GD11800]* was purchased from the Vienna *Drosophila* Resource Center (VDRC; Vienna, Austria). *Vps16A[d32]*, *Syx17[LL06330]* and *UVRAG[LL03097]*, *UVRAG[B21]*, and *UAS-GFP-FYVE* lines were described earlier (Wucherpfennig et al., 2003; Juhasz et al., 2008; Lee et al., 2011; Takats et al., 2013, 2014). The *FRT40A Mon1[d4]*, *UAS-Mon1-HA*, and *UAS-Ccz1-EosFP* stocks were kindly provided by Thomas Klein (Heinrich Heine University, Düsseldorf, Germany). We generated Gal4-expressing fat cell clones using *hs-Flp[22]*; *dLamp-3xmCherry*, *UAS-GFP*; *Act>CD2>Gal4*, *UAS-Dcr2* and positively marked mutant clones using the lines *hs-Flp*; *FRT40A tub-QS*; *et49-QF*, *QUAS-mCD8-GFP[5B]* and *hs-Flp[22]*; *QUAS-mCD8-GFP[5J]*; *ET49-QF*, *FRT82B tub-QS[21]/TM6* (all QF, QS, and QUAS transgenes came from BDSC). For the analysis of negatively marked mutant clones, we used the genotypes *hs-Flp[22]*; *Fb-Gal4*, *FRT40A UAS-dsRed* and *hs-Flp[22]*; *Fb-Gal4*, *UAS LAMP1-GFP*, *FRT40A UAS-dsRed* and *hs-Flp[22]*; *Fb-Gal4*, *FRT40A UAS-GFP*. For two experiments with *Rab5[d2]* mutant clones, we used clonal systems without a mutant cell marker: *hs-Flp[22]*; *Fb-Gal4*, *UAS-LAMP1-GFP*, *FRT40A* and *hs-Flp[22]*; *Fb-Gal4*, *FRT40A*; *UAS-GFP-Rab7*. Because fat cells

homozygous mutant for *Rab5[d2]* are larger than control cells and have a bigger nucleus, these cells can be easily identified without using an additional marker. Detailed genotype information is shown in Supplemental Table S1.

Molecular cloning and generation of transgenic animals

For generating N-terminally 3xmCherry tagged Atg8a under the control of the endogenous Atg8a promoter and containing all introns and 3' UTR, mCherry coding sequence was amplified from UAS-mCherry-GGG vector (kindly provided by Thomas Neufeld, University of Minnesota, Minneapolis, MN) by using primers AGAG-GTACCAGAAGGGTGGCGGAAGTGGCATGGTGAGCAAGGGC-GAGGA and TCCGGTACCCGGATCCACCTCCCTTGACAGCTC-GTCCATGCCG. The resulting PCR fragment was cut with *Acc65I* and cloned into a *BsrGI* site located at the end of mCherry coding sequence in the UAS-mCherry-GGG vector. By repeating another round of cloning on the resulting vector, a tandem 3xmCherry vector was made. Then a 1700-base pair fragment upstream of the translation start ATG sequence was amplified from the genomic Atg8a locus using primers GACTGAATTCGATTGCAATGAAGAG-GTAATTGGC and GAGCAGCATGCCAATGTGATTGAT. This extended Atg8a promoter region was cloned into our 3xmCherry vector as an *SphI-EcoRI* fragment, replacing the UAS sequences and minimal Hsp70 promoter. Finally, the genomic region of Atg8a was PCR amplified using the primers CTCGAGGTACCAAACTGC-GAGGCCAACGAAC and TATAGCGGCCGCGGAGGTGGCATGAGTTCCAATACAAGGAGGAGCA and cloned as a *NotI-Acc65I* fragment into our new vector to generate pAtg8apromoter-3xmCherry-Atg8a. To clone the genomic promoter-driven, C-terminally 3xmCherry-tagged dLamp reporter, the *Drosophila* Lamp locus was PCR amplified, including 403 base pairs upstream of the translation start ATG codon, using primers TATATCAATTGCATGCTGCAG-TTTCCTGTGTTATAAACCCCTGTGTG and catctgaattcGAAGCT-CATGTAACCGCGGGAG. This PCR product was cut into two fragments by *SphI-EcoRI* digestion (this gene contains an *SphI* digestion site 854 base pairs downstream of the translation start codon). The 3' fragment was ligated into an *SphI-EcoRI*-digested UAS-3xmCherry-GGG vector, replacing UAS sequences and the Hsp70 promoter. Then a 5' *SphI* fragment was inserted into the partial 3' Lamp-3xmCherry construct *SphI* to yield pdLamppromoter-dLamp-3xmCherry. The tubulin promoter-driven, N-terminally GFP-tagged p62 construct was made by cloning a 518-base pair promoter region upstream of the translation start codon of alphaTub84B gene using primers GTATGCGGCCGCATGCAAGGGAGAGGGGAAGTTATG-GAGTT and TATAGCGGCCGCTGCCGAATTCATTGAGTTTTATT-GGAAGTGTTCACACG as an *SphI-EcoRI* fragment into pUAST, replacing UAS sequences and the Hsp70 promoter. GFP-p62 coding sequences were cut out from pUAS-GFP-p62 (Chang and Neufeld, 2009) and inserted downstream of the tubulin promoter using *NotI* and *XbaI*. To generate genomic promoter-driven, C-terminally 3xHA-tagged Atg14 rescue transgene, we first replaced the *EcoRI-Acc65I* mCherry coding fragment in our pGen3xmCherry vector (Takats et al., 2014) with that of 3xHA annealed from synthetic oligos. Next we amplified the Atg14 locus, including the promoter region 629 base pairs upstream of the translation start codon, using GGCGCGCCGCATGCGGCCGCCCATGCCCTATGC-CAAGAC and TCTAGAGCTAGCGGTACCTTTGATCCAGCGCAG-CACCGA. This fragment was cloned into pGen3xHA upstream of the 3xHA sequence after *NotI-Acc65I* digestion. To generate a double gRNA construct to target the Atg14 locus, two pairs of oligos (CTTCGCTTGACAGCTTTCGTCGGAGC, AAACGCTCCGAC-GAAAGCTGCAAGC and CTTCGAGCGCTCCACAAACGGCG,

AAACCGCCGTTTGTGGAGGCGCTC) were annealed and cloned into the pBFv-U6.2B vector as described (Kondo and Ueda, 2013). Stable transgenic fly lines were established by microinjection of *Drosophila* embryos for all constructs (BestGene, Chino Hills, CA).

Histology, imaging, and statistics

For LTR staining, we dissected and incubated the fat body from 4-h-starved early L3-stage larvae for 5 min in 100 nM LTR (Invitrogen, Budapest, Hungary) diluted in phosphate-buffered saline (PBS). Then we transferred specimens to mounting solution (0.2 µg/ml 4',6-diamidino-2-phenylindole in a 1:1 mixture of PBS and glycerin). Magic Red staining was performed as described (Mauvezin et al., 2015). For immunostaining of developing eyes, late-L3-stage wandering larvae were inverted and fixed for 30 min in 3.7% paraformaldehyde in PBS at room temperature. Specimens were washed for 3 × 20 min in PBTX-DOC buffer (0.1% Triton X-100 and 0.5% sodium deoxycholate in PBS) and incubated overnight in 10% goat serum-containing PBTX-DOC at 4°C. Specimens were transferred to primary antibody solution diluted in 5% goat serum-containing PBTX-DOC for 90 min at room temperature. After 3 × 20 min washes in PBTX-DOC, specimens were incubated in secondary antibody solution diluted in 5% goat serum-containing PBTX-DOC for 90 min at room temperature. Finally, specimens were washed once in PBTX-DOC and twice in PBS and mounted as described. The protocol for immunostaining of 4-h-starved early-L3 larval fat bodies was described earlier (Takats et al., 2013). We used the primary antibodies rabbit anti-Boss (1:1000; Sevrioukov et al., 1999), mouse anti-Notch (1:50; C458.2H-c; Developmental Studies Hybridoma Bank [DSHB], Iowa City, Iowa), rat anti-Atg8a (1:300; Takats et al., 2013), and rabbit anti-Rab7 (1:500; Tanaka and Nakamura, 2008) and the secondary antibodies Alexa Fluor 488-, 568-, and 647-conjugated anti-rabbit, anti-rat, and anti-mouse (all 1:1500; Invitrogen). Pictures were taken using a Zeiss Axio Imager M2 microscope equipped with an Apotome2 grid confocal unit and AxioCam MRm. We quantified fluorescence structures from original, unmodified pictures using ImageJ (National Institutes of Health, Bethesda, MD). The threshold was set manually by the same person working in a darkroom. The quantified data were evaluated by performing the appropriate statistical tests as described previously (Takats et al., 2013, 2014).

Biochemistry

For Y2H assays, Mon1 and Ccz1 cDNAs were amplified using the primer pairs ATGGAAGTAGAGCAGACGTCAGTCAG and TTAGAATGTGGCATGGTTTCGTATAAA, and ATGGCTAAATTATGCAACGCGTA and TTATTTGTCAAAAAATACATCATCTGTGAGC, respectively. Rab5, Rab7, and Rab11 constitutive active and dominant negative versions were amplified using genomic DNA extracted from transgenic fly stocks. The primer pairs ATGGCAACCACTCACGCAGCG and TCACTTGACAGCAGTTGTCGTCG were used for Rab5, ATGTCCGGACGTAAGAAATCC and TTAGCACTGACAGTTGTCAGGA for Rab7, and ATGGGTGCAAGAGAAGACGAGTA and TCACTGACAGCACTGTTTGCG for Rab11. The fragments were cloned into pGADT7 AD (Gal4 DNA-activation domain) and pGBKT7 BD (Gal4 DNA-binding domain) vectors (Clontech/Central European Biosystems, Budapest, Hungary) and then transformed into the yeast strain PJ69-4A using the Frozen-EZ Yeast Transformation II kit (Zymo Research/Biocenter, Szeged, Hungary). The transformants were selected by growth in minimal medium (Trp⁻, Leu⁻), and to assay activation of the reporter gene and hence interaction, transformants were selected by growth on Trp⁻, Leu⁻, Ade⁻ plates. Empty vectors were used as negative controls. At least three colonies were checked for interaction for each transformation.

For the protein-lipid overlay assay, recombinant *Drosophila* Mon1 protein was cloned into the pET15b vector and expressed in *Escherichia coli* Rosetta cells (Millipore/Biocenter, Szeged, Hungary) and purified as described (Takats et al., 2013). The manufacturer's instructions were followed for the PIP Strips Membrane (Invitrogen, Budapest, Hungary) experiment.

Western blotting was carried out as described before (Pircs et al., 2012; Takats et al., 2013). Primary antibodies were rabbit anti-Rab7 (1:5000; Tanaka and Nakamura, 2008), rabbit anti-p62 (1:5000; Pircs et al., 2012), rabbit anti-Atg8a (1:5000; Takats et al., 2013), rabbit anti-cathepsin L (1:500; ab58991; Abcam, Cambridge, MA), and mouse anti-tubulin (1:1000; AA4.3; DSHB). Secondary antibodies were alkaline phosphatase-conjugated anti-rabbit and anti-mouse (both 1:5000; Sigma-Aldrich, Budapest Hungary).

Electron microscopy

Dissected fat bodies were processed for ultrastructural analysis as before (Takats et al., 2013). For correlative light and electron microscopy, fat bodies were adhered to a poly-L-lysine-coated glass slide in a drop of PBS. Images were taken by a fluorescence microscope in different magnifications to facilitate subsequent recognition of the fat body region containing the clone cells. Then fat bodies were fixed and embedded on the slide. Embedded clones were located in semithick sections stained with toluidine blue, followed by ultra-sectioning. Images were taken by a JEOL JEM-1011 transmission electron microscope equipped with an Olympus Morada camera and iTEM software.

ACKNOWLEDGMENTS

We thank Sarolta Pálfi for technical assistance and colleagues and stock centers listed in the *Materials and Methods* section for providing reagents. This work was supported by the Wellcome Trust (087518/Z/08/A to G.J.), the Hungarian Scientific Research Fund (PD112632 to K.H.), and the Hungarian Academy of Sciences (Lendület LP2014-2 to G.J.).

REFERENCES

- Bucci C, Thomsen P, Nicoziani P, McCarthy J, van Deurs B (2000). Rab7: a key to lysosome biogenesis. *Mol Biol Cell* 11, 467–480.
- Cabrera M, Nordmann M, Perz A, Schmedt D, Gerondopoulos A, Barr F, Piehler J, Engelbrecht-Vandre S, Ungermann C (2014). The Mon1-Ccz1 GEF activates the Rab7 GTPase Ypt7 via a longin-fold-Rab interface and association with PI3P-positive membranes. *J Cell Sci* 127, 1043–1051.
- Chang YY, Neufeld TP (2009). An Atg1/Atg13 complex with multiple roles in TOR-mediated autophagy regulation. *Mol Biol Cell* 20, 2004–2014.
- Chen Y, Zhou F, Zou S, Yu S, Li S, Li D, Song J, Li H, He Z, Hu B, et al. (2014). A Vps21 endocytic module regulates autophagy. *Mol Biol Cell* 25, 3166–3177.
- Cherry S, Jin EJ, Ozel MN, Lu Z, Agi E, Wang D, Jung WH, Epstein D, Meinerzhagen IA, Chan CC, et al. (2013). Charcot-Marie-Tooth 2B mutations in rab7 cause dosage-dependent neurodegeneration due to partial loss of function. *Elife* 2, e01064.
- Cui Y, Zhao Q, Gao C, Ding Y, Zeng Y, Ueda T, Nakano A, Jiang L (2014). Activation of the Rab7 GTPase by the MON1-CCZ1 complex is essential for PVC-to-vacuole trafficking and plant growth in Arabidopsis. *Plant Cell* 26, 2080–2097.
- Diao J, Liu R, Rong Y, Zhao M, Zhang J, Lai Y, Zhou Q, Wilz LM, Li J, Vivona S, et al. (2015). ATG14 promotes membrane tethering and fusion of autophagosomes to endolysosomes. *Nature* 520, 563–566.
- Dilcher M, Kohler B, von Mollard GF (2001). Genetic interactions with the yeast Q-SNARE Vti1 reveal novel functions for the R-SNARE Ykt6. *J Biol Chem* 276, 34537–34544.
- Dooley HC, Razi M, Polson HE, Girardin SE, Wilson MI, Tooze SA (2014). WIP2 links LC3 conjugation with PI3P, autophagosome formation, and pathogen clearance by recruiting Atg12–5–16L1. *Mol Cell* 55, 238–252.
- Fader CM, Colombo MI (2009). Autophagy and multivesicular bodies: two closely related partners. *Cell Death Differ* 16, 70–78.

- Filimonenko M, Stuffers S, Raiborg C, Yamamoto A, Malerod L, Fisher EM, Isaacs A, Brech A, Stenmark H, Simonsen A (2007). Functional multivesicular bodies are required for autophagic clearance of protein aggregates associated with neurodegenerative disease. *J Cell Biol* 179, 485–500.
- Gerondopoulos A, Langemeyer L, Liang JR, Linford A, Barr FA (2012). BLOC-3 mutated in Hermansky-Pudlak syndrome is a Rab32/38 guanine nucleotide exchange factor. *Curr Biol* 22, 2135–2139.
- Gutierrez MG, Munafo DB, Beron W, Colombo MI (2004). Rab7 is required for the normal progression of the autophagic pathway in mammalian cells. *J Cell Sci* 117, 2687–2697.
- Hennig KM, Colombani J, Neufeld TP (2006). TOR coordinates bulk and targeted endocytosis in the *Drosophila melanogaster* fat body to regulate cell growth. *J Cell Biol* 173, 963–974.
- Hickey CM, Stroupe C, Wickner W (2009). The major role of the Rab Ypt7p in vacuole fusion is supporting HOPS membrane association. *J Biol Chem* 284, 16118–16125.
- Ishihara N, Hamasaki M, Yokota S, Suzuki K, Kamada Y, Kihara A, Yoshimori T, Noda T, Ohsumi Y (2001). Autophagosome requires specific early Sec proteins for its formation and NSF/SNARE for vacuolar fusion. *Mol Biol Cell* 12, 3690–3702.
- Itakura E, Kishi C, Inoue K, Mizushima N (2008). Beclin 1 forms two distinct phosphatidylinositol 3-kinase complexes with mammalian Atg14 and UVRAG. *Mol Biol Cell* 19, 5360–5372.
- Itakura E, Kishi-Itakura C, Mizushima N (2012). The hairpin-type tail-anchored SNARE syntaxin 17 targets to autophagosomes for fusion with endosomes/lysosomes. *Cell* 151, 1256–1269.
- Jiang P, Nishimura T, Sakamaki Y, Itakura E, Hatta T, Natsume T, Mizushima N (2014). The HOPS complex mediates autophagosome-lysosome fusion through interaction with syntaxin 17. *Mol Biol Cell* 25, 1327–1337.
- Juhász G, Hill JH, Yan Y, Sass M, Baehrecke EH, Backer JM, Neufeld TP (2008). The class III PI(3)K Vps34 promotes autophagy and endocytosis but not TOR signaling in *Drosophila*. *J Cell Biol* 181, 655–666.
- Kim J, Dalton VM, Eggerton KP, Scott SV, Klionsky DJ (1999). Apg7p/Cvt2p is required for the cytoplasm-to-vacuole targeting, macroautophagy, and peroxisome degradation pathways. *Mol Biol Cell* 10, 1337–1351.
- Kondo S, Ueda R (2013). Highly improved gene targeting by germline-specific Cas9 expression in *Drosophila*. *Genetics* 195, 715–721.
- Kucharczyk R, Kierzek AM, Slonimski PP, Rytka J (2001). The Ccz1 protein interacts with Ypt7 GTPase during fusion of multiple transport intermediates with the vacuole in *S. cerevisiae*. *J Cell Sci* 114, 3137–3145.
- Lee G, Liang C, Park G, Jang C, Jung JU, Chung J (2011). UVRAG is required for organ rotation by regulating Notch endocytosis in *Drosophila*. *Dev Biol* 356, 588–597.
- Liang C, Feng P, Ku B, Dotan I, Canaani D, Oh BH, Jung JU (2006). Autophagic and tumour suppressor activity of a novel Beclin1-binding protein UVRAG. *Nat Cell Biol* 8, 688–699.
- Lindmo K, Stenmark H (2006). Regulation of membrane traffic by phosphoinositide 3-kinases. *J Cell Sci* 119, 605–614.
- Lu H, Bilder D (2005). Endocytic control of epithelial polarity and proliferation in *Drosophila*. *Nat Cell Biol* 7, 1232–1239.
- Matsunaga K, Saitoh T, Tabata K, Omori H, Satoh T, Kurotori N, Maejima I, Shirahama-Noda K, Ichimura T, Isobe T, et al. (2009). Two Beclin 1-binding proteins, Atg14L and Rubicon, reciprocally regulate autophagy at different stages. *Nat Cell Biol* 11, 385–396.
- Mauvezin C, Ayala C, Braden CR, Kim J, Neufeld TP (2014). Assays to monitor autophagy in *Drosophila*. *Methods* 68, 134–139.
- Mauvezin C, Nagy P, Juhász G, Neufeld TP (2015). Autophagosome-lysosome fusion is independent of V-ATPase-mediated acidification. *Nat Commun* 6, 7007.
- McEwan DG, Popovic D, Gubas A, Terawaki S, Suzuki H, Stadel D, Coxon FP, Miranda de Stegmann D, Bhogaraju S, Maddi K, et al. (2015). PLEKHM1 regulates autophagosome-lysosome fusion through HOPS complex and LC3/GABARAP proteins. *Mol Cell* 57, 39–54.
- Mizushima N, Levine B, Cuervo AM, Klionsky DJ (2008). Autophagy fights disease through cellular self-digestion. *Nature* 451, 1069–1075.
- Nagy P, Varga A, Kovacs AL, Takats S, Juhász G (2015). How and why to study autophagy in *Drosophila*: it's more than just a garbage chute. *Methods* 75, 151–161.
- Nezis IP, Simonsen A, Sagana AP, Finley K, Gaumer S, Contamine D, Rusten TE, Stenmark H, Brech A (2008). Ref(2)P, the *Drosophila melanogaster* homologue of mammalian p62, is required for the formation of protein aggregates in adult brain. *J Cell Biol* 180, 1065–1071.
- Nordmann M, Cabrera M, Perz A, Brocker C, Ostrowicz C, Engelbrecht-Vandre S, Ungermann C (2010). The Mon1-Ccz1 complex is the GEF of the late endosomal Rab7 homolog Ypt7. *Curr Biol* 20, 1654–1659.
- Obara K, Sekito T, Ohsumi Y (2006). Assortment of phosphatidylinositol 3-kinase complexes-Atg14p directs association of complex I to the pre-autophagosomal structure in *Saccharomyces cerevisiae*. *Mol Biol Cell* 17, 1527–1539.
- Ohashi Y, Munro S (2010). Membrane delivery to the yeast autophagosome from the Golgi-endosomal system. *Mol Biol Cell* 21, 3998–4008.
- Pereira-Leal JB, Seabra MC (2001). Evolution of the Rab family of small GTP-binding proteins. *J Mol Biol* 313, 889–901.
- Pircs K, Nagy P, Varga A, Venkei Z, Erdi B, Hegedus K, Juhász G (2012). Advantages and limitations of different p62-based assays for estimating autophagic activity in *Drosophila*. *PLoS One* 7, e44214.
- Poteryaev D, Datta S, Ackema K, Zerial M, Spang A (2010). Identification of the switch in early-to-late endosome transition. *Cell* 141, 497–508.
- Pulipparacharuvil S, Akbar MA, Ray S, Sevrioukov EA, Haberman AS, Rohrer J, Kramer H (2005). *Drosophila* Vps16A is required for trafficking to lysosomes and biogenesis of pigment granules. *J Cell Sci* 118, 3663–3673.
- Ravikumar B, Imarisio S, Sarkar S, O'Kane CJ, Rubinsztein DC (2008). Rab5 modulates aggregation and toxicity of mutant huntingtin through macroautophagy in cell and fly models of Huntington disease. *J Cell Sci* 121, 1649–1660.
- Rieder SE, Emr SD (1997). A novel RING finger protein complex essential for a late step in protein transport to the yeast vacuole. *Mol Biol Cell* 8, 2307–2327.
- Rusten TE, Vaccari T, Lindmo K, Rodahl LM, Nezis IP, Sem-Jacobsen C, Wendler F, Vincent JP, Brech A, Bilder D, et al. (2007). ESCRTs and Fab1 regulate distinct steps of autophagy. *Curr Biol* 17, 1817–1825.
- Sevrioukov EA, He JP, Moghrabi N, Sunio A, Kramer H (1999). A role for the deep orange and carnation eye color genes in lysosomal delivery in *Drosophila*. *Mol Cell* 4, 479–486.
- Stenmark H (2009). Rab GTPases as coordinators of vesicle traffic. *Nat Rev Mol Cell Biol* 10, 513–525.
- Stroupe C, Collins KM, Fratti RA, Wickner W (2006). Purification of active HOPS complex reveals its affinities for phosphoinositides and the SNARE Vam7p. *EMBO J* 25, 1579–1589.
- Takats S, Nagy P, Varga A, Pircs K, Karpati M, Varga K, Kovacs AL, Hegedus K, Juhász G (2013). Autophagosomal Syntaxin17-dependent lysosomal degradation maintains neuronal function in *Drosophila*. *J Cell Biol* 201, 531–539.
- Takats S, Pircs K, Nagy P, Varga A, Karpati M, Hegedus K, Kramer H, Kovacs AL, Sass M, Juhász G (2014). Interaction of the HOPS complex with Syntaxin 17 mediates autophagosome clearance in *Drosophila*. *Mol Biol Cell* 25, 1338–1354.
- Tanaka T, Nakamura A (2008). The endocytic pathway acts downstream of Oskar in *Drosophila* germ plasm assembly. *Development* 135, 1107–1117.
- Wang CW, Stromhaug PE, Shima J, Klionsky DJ (2002). The Ccz1-Mon1 protein complex is required for the late step of multiple vacuole delivery pathways. *J Biol Chem* 277, 47917–47927.
- Wucherpfennig T, Wilsch-Brauninger M, Gonzalez-Gaitan M (2003). Role of *Drosophila* Rab5 during endosomal trafficking at the synapse and evoked neurotransmitter release. *J Cell Biol* 161, 609–624.
- Yousefian J, Troost T, Grawe F, Sasamura T, Fortini M, Klein T (2013). Dmon1 controls recruitment of Rab7 to maturing endosomes in *Drosophila*. *J Cell Sci* 126, 1583–1594.
- Zeigerer A, Gilleron J, Bogorad RL, Marsico G, Nonaka H, Seifert S, Epstein-Barash H, Kuchimanchi S, Peng CG, Ruda VM, et al. (2012). Rab5 is necessary for the biogenesis of the endolysosomal system in vivo. *Nature* 485, 465–470.